Analysis of flux-integrated semiexclusive cross sections for charged-current quasielastic neutrino scattering off ^{40}Ar at energies available at the MicroBooNE experiment

A. V. Butkevich[ORCID]

Institute for Nuclear Research, Russian Academy of Sciences, Moscow 117312, Russia

Flux-integrated semiexclusive differential and integral cross sections for quasielastic neutrino charged-current scattering on argon are analyzed. The cross sections are calculated using the relativistic distorted-wave impulse approximation and compare with recent MicroBooNE data. I found that the measured cross sections can be described well within the experimental uncertainties with value of the nucleon axial mass $1 < M_A < 1.2$ GeV. The contribution of the exclusive channel $(\nu_\mu, \mu p)$ to the flux-integrated inclusive cross sections is about 50%.

I. INTRODUCTION

Current [1,2] and future [3,4] neutrino oscillation experiments use high-intensity muon-(anti)neutrino beams that are not monoenergetic and peak in the energy range from tens of MeV to a few GeV. The goal of these experiments is to measure oscillation features in the neutrino energy spectrum reconstructed at far detectors. To evaluate the oscillation parameters, the probabilities of neutrino oscillations as functions of neutrino energy are measured. The accuracy to which they can extract neutrino oscillation parameters depends on their ability to determine the individual energy of detected neutrino. This requires detailed understanding of neutrino interactions with nuclei [5].

In the energy range $\varepsilon_\nu \sim 0.2-5$ GeV charged-current (CC) quasielastic (QE) scattering and scattering induced by two-body meson exchange current (MEC), resonance production, and deep inelastic process yield the main contributions to the neutrino-nucleus interaction. The understanding of these interactions comes through cross sections measurements on various channels. The incident neutrino energy can be reconstructed using the calorimetric method, which rely not only on the lepton and hadron energies visible in the final state after the neutrino has interacted but also on models of the neutrino-nucleus interactions that are implemented in neutrino events generators.

The CCQE interaction forms a significant contribution in many accelerator-based neutrino experiments [6–14]. Because the CCQE interaction represents a two particle scattering process (the residual nucleus is not detected), its final state

topology is simple with an easy identifiable lepton, and neutrino energy may be estimated using the outgoing lepton kinematics, i.e., applying kinematical methods. However, as neutrino beams have broad energy distributions, various contributions to the inclusive cross section, where only final lepton is detected, can significantly overlap with each other making it difficult to identify the channels of neutrino interaction. The interpretation of the inclusive CCQE data is complicated because of the presence of other interactions such as MEC and pion production, where the pion is absorbed in the residual nucleus. So, when only the muon is detected, the event can easily be mistaken as a CCQE interaction and application of the kinematic method will lead to a bias in the neutrino energy estimation.

Compared to inclusive experiments, semiexclusive scattering $(\nu_\mu, \mu p)$ provides additional information about hadrons in the final state. In this process the neutrino removes a single intact nucleon from the nucleus without production of any additional particles. For these $(\nu_\mu, \mu p)$ events the experimental signature requires the identification of a neutrino interaction vertex with an outgoing lepton, exactly one outgoing proton, and no additional particles, which is relatively straight forward to measure. The information about hadrons will improve the accuracy of reconstruction of the incoming neutrino energy. Understanding the interaction of neutrino with argon nuclei is of particular importance, since neutrino oscillation experiments such as DUNE [3] and SBN [15] employ neutrino detectors using liquid argon time projector chamber (LArTPs).

Weak interactions of neutrinos probe the nucleus in a similar way as electromagnetic electron interactions. Of course, there are a number of differences with neutrino scattering, the most important one being the absence of the axial current contribution. Nevertheless the influence of the nuclear medium is the same as in neutrino-nucleus scattering data. Precise electron-scattering data gives a unique opportunity to validate the nuclear model employed in neutrino physics. Therefore, the detailed comparison with $(e, e'p)$ data is a necessary test

for any theoretical model used to describe the CC1p0π cross sections.

Systematic measurements of $(e, e'p)$ cross sections were performed at Saclay [16], NIKHEF [17], and Jefferson Laboratory (JLab) [18–20]. The impact of the MEC on the nuclear response functions and differential cross section for the knockout of protons from ^{16}O was studied in Ref. [18]. It was shown that explicit inclusion of the two-body current contribution does not markedly improve the overall agreement between the data and calculated cross sections. Unfortunately, the cross section data for the semi-exclusive lepton scattering on argon in the relevant energy range are rather scare. There are only experimental data for $\approx$2.2 GeV electron scattering of ^{40}Ar [20] and flux-integrated differential CCQE-like cross sections for ν_μ ^{40}Ar scattering with the detection of a proton in the final state (CC1p0π), measured with the MicroBooNE detector [13]. On the other hand ^{40}Ca and ^{40}Ar nuclei have similar structures, and for calcium high resolution exclusive $(e, e'p)$ experiments were carried out at Tokyo [21,22], Saclay [23], and NIKHEF [24–26].

The data analysis of $(e, e'p)$ and $(\nu_\mu, \mu p)$ processes was performed in Refs. [18,27–32] within the relativistic distorted-wave impulse approximation (RDWIA) [33–35], using a relativistic shell model approach. The implementation of the final state interaction (FSI) of the ejected nucleon has been done differently. The RDWIA approach describes with high degree of accuracy the experimental shape of the outgoing particle momentum distributions. In order to reproduce experimental cross sections, normalizations of the bound-state wave functions were fit to the data and identified with the spectroscopic factors. The semi-inclusive process for CCQE reactions was recently discussed in Refs. [36–38].

In this work the flux-integrated differential cross sections of ^{40}Ar($\nu_\mu, \mu p$) interactions are calculated with the RDWIA approach, using the Booster Neutrino Beam (BNB) at Fermilab [39]. This approach was successfully applied in Refs. [40–45] for calculation of the CCQE semiexclusive and inclusive cross sections for the electron and neutrino scattering on ^{12}C, ^{16}O, ^{40}Ca, and ^{40}Ar nuclei. The aim of this work is to test the RDWIA predictions against the MicroBooNE data [13]. Within this model the range of the values of nucleon axial mass from the measured CC1p0π flux-integrated differential cross sections is estimated.

The outline of this article is as follows. In Sec. II I present briefly the formalism for the CCQE semi-inclusive scattering process and basic aspects of the RDWIA approach, used for the calculation. The results are presented and discussed in Sec. III. The conclusions are summarized in Sec. IV.

II. FORMALISM OF QUASIELASTIC SCATTERING AND RDWIA

In this section, I consider shortly the formalism used to describe electron and neutrino quasielastic exclusive

$$l(k_i) + A(p_A) \rightarrow l'(k_f) + N(p_x) + B(p_B) \quad (1)$$

and inclusive

$$l(k_i) + A(p_A) \rightarrow l'(k_f) + X \quad (2)$$

scattering off nuclei in the one-photon (W-boson) exchange approximation. Here, l labels the incident lepton [electron or muon (anti)neutrino], and l' represents the scattered lepton (electron or muon), $k_i = (\varepsilon_i, \boldsymbol{k}_i)$ and $k_f = (\varepsilon_f, \boldsymbol{k}_f)$ are the initial and final lepton momenta, $p_A = (\varepsilon_A, \boldsymbol{p}_A)$, and $p_B = (\varepsilon_B, \boldsymbol{p}_B)$ are the initial and final target momenta, $p_x = (\varepsilon_x, \boldsymbol{p}_x)$ is the ejectile nucleon momentum, $q = (\omega, \boldsymbol{q})$ is the momentum transfer carried by the virtual photon (W-boson), and $Q^2 = -q^2 = \boldsymbol{q}^2 - \omega^2$ is the photon (W-boson) virtuality.

A. CCQE lepton-nucleus cross sections

In the laboratory frame the differential cross section for exclusive electron (σ^{el}) and (anti)neutrino (σ^{cc}) CC scattering can be written as

$$\frac{d^6\sigma^{el}}{d\varepsilon_f d\Omega_f d\varepsilon_x d\Omega_x} = \frac{|\boldsymbol{p}_x|\varepsilon_x}{(2\pi)^3} \frac{\varepsilon_f}{\varepsilon_i} \frac{\alpha^2}{Q^4} L_{\mu\nu}^{(el)} \mathcal{W}^{\mu\nu(el)}, \quad (3a)$$

$$\frac{d^6\sigma^{cc}}{d\varepsilon_f d\Omega_f d\varepsilon_x d\Omega_x} = \frac{|\boldsymbol{p}_x|\varepsilon_x}{(2\pi)^5} \frac{|\boldsymbol{k}_f|}{\varepsilon_i} \frac{G^2 \cos^2\theta_c}{2} L_{\mu\nu}^{(cc)} \mathcal{W}^{\mu\nu(cc)}, \quad (3b)$$

where Ω_f is the solid angle for the lepton momentum, Ω_x is the solid angle for the ejectile nucleon momentum, $\alpha \simeq 1/137$ is the fine-structure constant, $G \simeq 1.16639 \times 10^{-11}$ MeV^{-2} is the Fermi constant, θ_C is the Cabbibo angle ($\cos\theta_C \approx 0.9749$), $L^{\mu\nu}$ is the lepton tensor, and $\mathcal{W}_{\mu\nu}^{(el)}$ and $\mathcal{W}_{\mu\nu}^{(cc)}$ are, correspondingly, the electromagnetic and weak CC nuclear tensors.

For exclusive reactions in which only a single discrete state or narrow resonance of the target is excited, it is possible to integrate over the peak in missing energy and obtain a fivefold differential cross section of the form

$$\frac{d^5\sigma^{el}}{d\varepsilon_f d\Omega_f d\Omega_x} = R \frac{|\boldsymbol{p}_x|\tilde{\varepsilon}_x}{(2\pi)^3} \frac{\varepsilon_f}{\varepsilon_i} \frac{\alpha^2}{Q^4} L_{\mu\nu}^{(el)} W^{\mu\nu(el)}, \quad (4a)$$

$$\frac{d^5\sigma^{cc}}{d\varepsilon_f d\Omega_f d\Omega_x} = R \frac{|\boldsymbol{p}_x|\tilde{\varepsilon}_x}{(2\pi)^5} \frac{|\boldsymbol{k}_f|}{\varepsilon_i} \frac{G^2 \cos^2\theta_c}{2} L_{\mu\nu}^{(cc)} W^{\mu\nu(cc)}, \quad (4b)$$

where R is a recoil factor

$$R = \int d\varepsilon_x \delta(\varepsilon_x + \varepsilon_B - \omega - m_A) = \left| 1 - \frac{\tilde{\varepsilon}_x}{\varepsilon_B} \frac{\boldsymbol{p}_x \cdot \boldsymbol{p}_B}{\boldsymbol{p}_x \cdot \boldsymbol{p}_x} \right|^{-1}, \quad (5)$$

$\tilde{\varepsilon}_x$ is solution to equation $\varepsilon_x + \varepsilon_B - m_A - \omega = 0$, where $\varepsilon_B = \sqrt{m_B^2 + \boldsymbol{p}_B^2}$, $\boldsymbol{p}_B = \boldsymbol{q} - \boldsymbol{p}_x$ and m_A and m_B are masses of the target and recoil nucleus, respectively. Note, that missing momentum is $\boldsymbol{p}_m = \boldsymbol{p}_x - \boldsymbol{q}$ and missing energy $\boldsymbol{\varepsilon}_m$ is defined by $\boldsymbol{\varepsilon}_m = m + m_B - m_A$. The differential cross sections $(d^3\sigma^{el(cc)}/d\varepsilon_f d\Omega_f)_{ex}$ can be obtained by integrating the exclusive cross sections (4a) and (4b) over solid angle for the ejectile nucleon.

All information about the nuclear structure and FSI effects is contained in the electromagnetic and weak CC hadronic tensors, $W_{\mu\nu}^{(el)}$ and $W_{\mu\nu}^{(cc)}$, which are given by the bilinear products of the transition matrix elements of the nuclear electromagnetic or CC operator $J_\mu^{(el)(cc)}$ between the initial nucleus state $|A\rangle$ and the final state $|B_f\rangle$ as

$$W_{\mu\nu}^{(el)(cc)} = \sum_f \langle B_f, p_x | J_\mu^{(el)(cc)} | A \rangle \langle A | J_\nu^{(el)(cc)\dagger} | B_f, p_x \rangle, \quad (6)$$

where the sum is taken over undetected states.

In the inclusive reaction (2) only the outgoing lepton is detected and lepton scattering cross sections in term of nuclear response functions can be written as

$$\frac{d^3\sigma^{el}}{d\varepsilon_f d\Omega_f} = \sigma_M \left(V_L R_L^{(el)} + V_T R_T^{(el)} \right), \tag{7a}$$

$$\frac{d^3\sigma^{cc}}{d\varepsilon_f d\Omega_f} = \frac{G^2 \cos^2\theta_c}{(2\pi)^2} \varepsilon_f |\mathbf{k}_f| (v_0 R_0 + v_T R_T + v_{zz} R_{zz}$$
$$- v_{0z} R_{0z} - h v_{xy} R_{xy}), \tag{7b}$$

where

$$\sigma_M = \frac{\alpha^2 \cos^2\theta/2}{4\varepsilon_i^2 \sin^4\theta/2} \tag{8}$$

is the Mott cross section and h is $+1$ for positive lepton helicity and -1 for negative lepton helicity. The coupling coefficient V_k and v_k, the expression of which are given in Ref. [40] are kinematic factors depending on the lepton's kinematics. The response functions R_i are given in terms of components of the inclusive hadronic tensors [40] and depend on the variables (Q^2, ω) or $(|\mathbf{q}|, \omega)$.

The experimental data of the $(e, e'p)$ reaction are usually presented in terms of the reduced cross section

$$\sigma_{red} = \frac{d^5\sigma}{d\varepsilon_f d\Omega_f d\Omega_x} / K^{(el)(cc)} \sigma_{lN}, \tag{9}$$

where $K^{el} = R p_x \varepsilon_x / (2\pi)^3$ and $K^{cc} = R p_x \varepsilon_x / (2\pi)^5$ are phase-space factors for electron and neutrino scattering and σ_{lN} is the corresponding elementary cross section for the lepton scattering from the moving free nucleon. The reduced cross section is an interesting quantity that can be regarded as the nucleon momentum distribution modified by FSI. Therefore these cross sections for (anti)neutrino scattering off nuclei are similar to the electron scattering apart from small differences at low beam energy due to effects of Coulomb distortion of the incoming electron wave function. Precise electron reduced cross section data can be used to validate the neutrino reduced cross sections employed in neutrino generators.

B. Model

I describe genuine QE electron-nuclear scattering within the RDWIA approach. This formalism is based on the impulse approximation (IA), assuming that the incoming lepton interacts with only one nucleon of the target, which is subsequently emitted. In this approximation the nuclear current is written as a sum of single-nucleon currents and the nuclear matrix element in Eq. (6) takes the form

$$\langle p, B | J^\mu | A \rangle = \int d^3r \exp(i\mathbf{t} \cdot \mathbf{r}) \overline{\Psi}^{(-)}(\mathbf{p}, \mathbf{r}) \Gamma^\mu \Phi(\mathbf{r}), \tag{10}$$

where Γ^μ is the vertex function, $\mathbf{t} = \varepsilon_B \mathbf{q} / W$ is the recoil-corrected momentum transfer, $W = \sqrt{(m_A + \omega)^2 - \mathbf{q}^2}$ is the invariant mass, and Φ and $\Psi^{(-)}$ are relativistic bound-state and outgoing wave functions.

For electron scattering, the CC2 electromagnetic vertex function for a free nucleon [46] is used:

$$\Gamma_V^\mu = F_V(Q^2)\gamma^\mu + i\sigma^{\mu\nu} \frac{q_\nu}{2m} F_M(Q^2), \tag{11}$$

where $\sigma^{\mu\nu} = i[\gamma^\mu, \gamma^\nu]/2$, F_V and F_M are the Dirac and Pauli nucleon form factors. The single-nucleon charged current has $V-A$ structure $J^{\mu(cc)} = J_V^\mu + J_A^\mu$. For a free-nucleon vertex function $\Gamma^{\mu(cc)} = \Gamma_V^\mu + \Gamma_A^\mu$ I use the CC2 vector current vertex function

$$\Gamma_V^\mu = F_V(Q^2)\gamma^\mu + i\sigma^{\mu\nu} \frac{q_\nu}{2m} F_M(Q^2) \tag{12}$$

and the axial current vertex function

$$\Gamma_A^\mu = F_A(Q^2)\gamma^\mu \gamma_5 + F_P(Q^2) q^\mu \gamma_5. \tag{13}$$

The weak vector form factors F_V and F_M are related to the corresponding electromagnetic form factors $F_V^{(el)}$ and $F_M^{(el)}$ for protons and neutrons by the hypothesis of the conserved vector current. The approximation of Ref. [47] is used for the Dirac and Pauli nucleon form factors. Because the bound nucleons are off-shell I employ the de Forest prescription [46] and Coulomb gauge for the off-shell vector current vertex Γ_V^μ. The vector-axial F_A and pseudoscalar F_P form factors are parametrized using a dipole approximation:

$$F_A(Q^2) = \frac{F_A(0)}{\left(1 + Q^2/M_A^2\right)^2}, \quad F_P(Q^2) = \frac{2m F_A(Q^2)}{m_\pi^2 + Q^2}, \tag{14}$$

where $F_A(0) = 1.2724$, M_A is the axial mass that controls Q^2 dependence of $F_A(Q^2)$, and m_π is the pion mass.

In the RDWIA calculations the independent particle shell model (IPSM) is assumed for the nuclear structure. In Eq. (10) the relativistic bound-state wave functions for nucleons Φ are obtained as the self-consistent solutions of a Dirac equation, derived within a relativistic mean-field approach from a Lagrangian containing σ, ω, and ρ mesons [48]. These functions were calculated by the TIMORA code [49] with the normalization factors S_α relative to full occupancy of the IPSM orbital α of ^{40}Ca. For ^{40}Ca and ^{40}Ar an average factor $\langle S \rangle \approx 87\%$. This estimation of depletion of hole states follows from the RDWIA analysis of ^{40}Ca$(e, e'p)$ data [43]. The source of the reduction of the $(e, e'p)$ spectroscopic factors with respect to the mean field values are the short-range and tensor correlations in the ground state, leading to the appearance of the high-momentum and high-energy component in the nucleon distribution in the target. There is as yet no rigorous, coherent theoretical picture that uniformly explains the data all missing energies and all missing momentum. Mean values of the proton and neutron binding energies and occupancies of shells are given also in Ref. [43]. In the RDWIA model, final state interaction effects for the outgoing nucleon are taken into account. The system of two coupled first-order Dirac equations is reduced to a single second-order Schrödinger-like equation for the upper component of the Dirac wave function Ψ. This equation contains equivalent nonrelativistic central and spin-orbit potentials which are functions of the relativistic, energy dependent, scalar, and vector optical potentials. The optical potential consists of a real part, which describes the rescattering of the ejected nucleon and an imaginary part
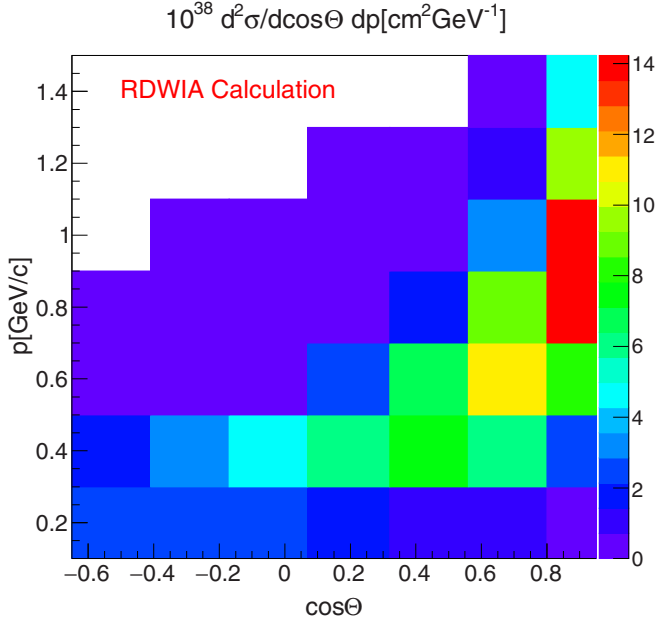
10^{38} $d^2\sigma/d\cos\Theta$ $dp[cm^2GeV^{-1}]$

FIG. 1. The flux-integrated double-differential CC1p0π cross section as a function of muon momentum and the cosine of the muon scattering angle.

FIG. 2. The flux-integrated semiexclusive CCQE $d^2\sigma/dp_\mu d\cos\theta$ cross section for ν_μ-^{40}Ar scattering as a function of p_μ for the four muon scattering angle bins: $\cos\theta = [(-0.65) - (-0.4)]$, $[(-0.4) - (-0.17)]$, $[(-0.17) - 0.07]$, and $(0.07 - 0.32)$. As shown in the key, cross sections were calculated with $M_A = 1$ GeV and 1.2 GeV.

which account for its absorption into unobserved channels. The LEA program [50] is used for the numerical calculation of the distorted wave functions with the EDAD1 parametrization [51] of the relativistic optical potential for calcium. This code was successfully tested in Ref. [43] against $A(e, e'p)$ data for electron scattering off ^{40}Ca. In Ref. [43] the reduced cross sections as functions of missing momentum calculated in the RDWIA approach for the ^{40}Ca$(e, e'p)$ reaction are shown in Figs. 1 and 2 with NIKHEF data and provide a good description of the measured distributions. Neutrino and antineutrino cross sections are also shown in Fig. 1 for comparison. The RDWIA calculations are generally expected to be more accurate at higher Q^2, since QE $(e, e'p)$ is expected to be dominated by single-particle interactions in this regime of four-momentum transfer and two-body currents stemming from meson-exchange currents are not needed to explain the data at this Q^2 [18]. In order to calculate the inclusive cross sections $(d\sigma/d\varepsilon_f d\Omega_f)_{RDWIA}$, I use the approach in which only the real part of the optical potential EDAD1 is included. The effect of the FSI on the inclusive cross section can be evaluated using the ratio

$$\Lambda(\varepsilon_f, \Omega_f) = \left(\frac{d^3\sigma}{d\varepsilon_f d\Omega_f}\right)_{RDWIA} \bigg/ \left(\frac{d^3\sigma}{d\varepsilon_f d\Omega_f}\right)_{PWIA}, \quad (15)$$

where $(d^3\sigma/d\varepsilon_f d\Omega_f)_{PWIA}$ is the result obtained in the plane-wave impulse approximation (PWIA). The inclusive cross sections with the FSI effects, taking into account short-range nucleon-nucleon (NN) correlations were calculated using the method proposed in Ref. [40] with the nucleon high-momentum and high-energy distribution from Ref. [52] that was renormalized to value of 13% for calcium and argon. The contribution of the NN-correlated pairs is evaluated in the
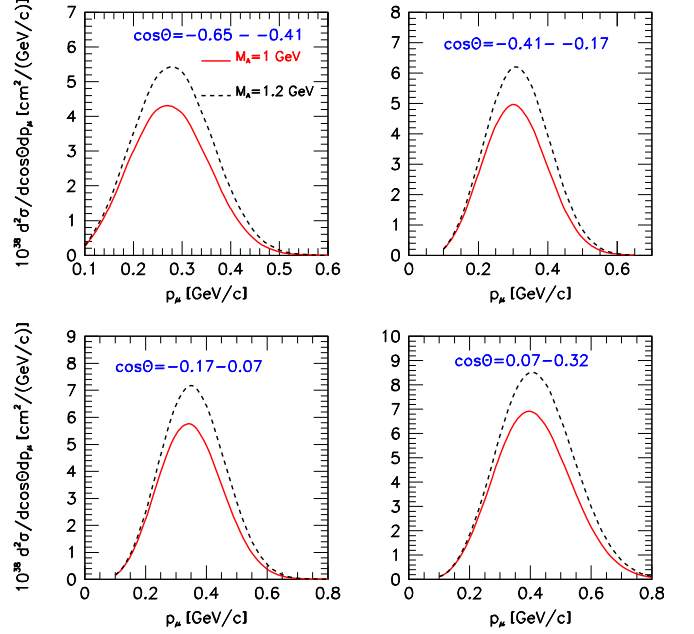
PWIA, i.e., the virtual photon couples to only one member of the NN pair. The FSI effects for the NN pair is estimated by scaling the PWIA result $(d^3\sigma/d\varepsilon_f d\Omega_f)_{NN}$ with $\Lambda(\varepsilon_f, \Omega_f)$ function. In Ref. [45] was shown that this approach describes well the electron scattering data for carbon, calcium, and argon at different kinematics. The calculated and measured cross sections are in agreement within the experimental uncertainties.

III. RESULTS AND ANALYSIS

The first measurement of exclusive CCQE-like neutrino-argon interaction cross sections, performed using the MicroBooNE liquid argon time projector chamber (LArTPC) neutrino detector was presented in Ref. [13]. A specific subset of CCQE-like interactions (CC1p0π interactions), includes CC ν_μ-^{40}Ar scattering events with a detected muon and exactly one proton, with momenta greater than 100 and 300 MeV/c, respectively. The selected CC1p0π event definition includes the beam-related background, i.e., events with any number of protons with momenta below 300 MeV/c, neutrons at any momenta, and charged pions with momentum lower than 70 MeV/c. This background is estimated from Monte Carlo simulation. The data were taken in a phase-space region that corresponds to $0.1 < p_\mu < 1.5$ GeV/c, $0.3 < p_p < 1$ GeV/c, $-0.65 < \cos\theta < 0.95$, and $\cos\theta_p > 0.15$. After the application of the event selection requirement only 410 CC1p0π candidate events were retained. The contribution of the beam-related background is about 12%.
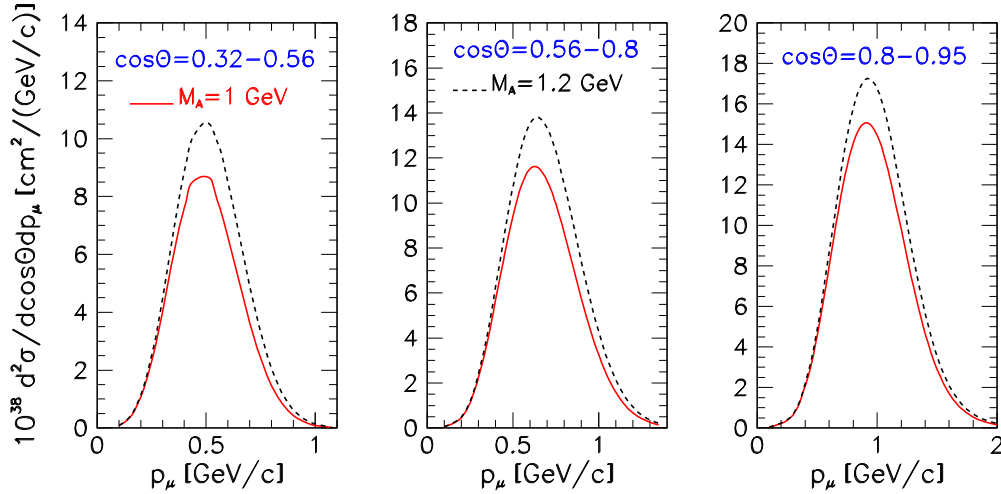
FIG. 3. Same as Fig. 2 but for muon scattering angle bins: $\cos\theta = (0.32–0.56)$, $(0.56–0.8)$, $(0.8–0.95)$.

A. Semiexclusive CCQE double differential cross section

For these CC1p0π events were measured the flux-integrated ν_μ-^{40}Ar differential cross sections in muon and proton momentum and angle, and as a function of the calorimetric measured energy and reconstructed momentum transfer. The statistical uncertainty of the integrated measured CC1p0π cross section is 15.9% and the systematic uncertainty sums to 26.2%. The MicroBooNE detector is located along the Booster Neutrino Beam (BNB) at Fermilab. The BNB energy spectrum extends to 2 GeV and peaks around 0.7 GeV [39]. In this work I calculate within the RDWIA model with $M_A = 1$ GeV and 1.2 GeV the flux-integrated CCQE semiexclusive cross sections, taking into account the MicroBooNE momentum thresholds for muons and protons. Thus, I do not consider MEC and NN-pair contributions nor the process where charged pions may be produced in the final state, because they are the beam-related background (three particles in the final state). The flux-integrated double-differential cross section $d^2\sigma/dp_\mu d\cos\theta$ of the semiexclusive CCQE ν_μ-^{40}Ar scattering is presented in Fig. 1, which shows the cross section as a function of muon momentum p_μ and muon scattering angle $\cos\theta$. Here, the result was obtained in the RDWIA approach with the value of the nucleon axial mass $M_A = 1$ GeV. The maximum of the calculated cross section is in the range $0.9 < p_\mu < 1.1$ GeV/c and $0.8 < \cos\theta < 0.96$. So, neutrino interactions with energy higher than 1 GeV and high values of $\cos\theta$ that corresponds to low momentum transfer, yield the main contribution to the measured cross sections.

Figures 2 and 3 show the flux-integrated $d^2\sigma/dp_\mu d\cos\theta$ cross sections as functions of p_μ for several bins of the muon scattering angle. On can observe that within the RDWIA model with $M_A = 1.2$ GeV the cross sections in the region of the QE peak are predicted to be on about 20% higher than cross sections calculated with $M_A = 1$ GeV.

B. Semiexclusive CCQE single differential cross section

Figure 4 shows the flux-integrated differential $d\sigma/d\cos\theta$ cross section as a function of the cosine of the measured muon scattering angle. In Ref. [13] was shown that the bin

migration effects on this measurement are small and within the assessed uncertainties. The data are compared to the RDWIA calculations. As can be seen in figure, calculated cross sections are in overall agreement with data, except for the highest $\cos\theta$ bin, where the measured cross section is lower than the theoretical predictions. Note, that in Ref. [13] the results of theoretical absolute cross section calculations using different event generators are also significantly higher than the measured cross section for this $\cos\theta$ bin.

As the differential $d\sigma/dp_\mu$, $d\sigma/dp_p$, and $d\sigma/dQ^2$ cross sections include contributions from all muon scattering angles, their agreement with the theoretical calculations is effected by these inclusions. In Ref. [13] the relevant cross sections in the case where events with $\cos\theta > 0.8$ are excluded and in the full available phase space $-0.65 < \cos\theta < 0.95$
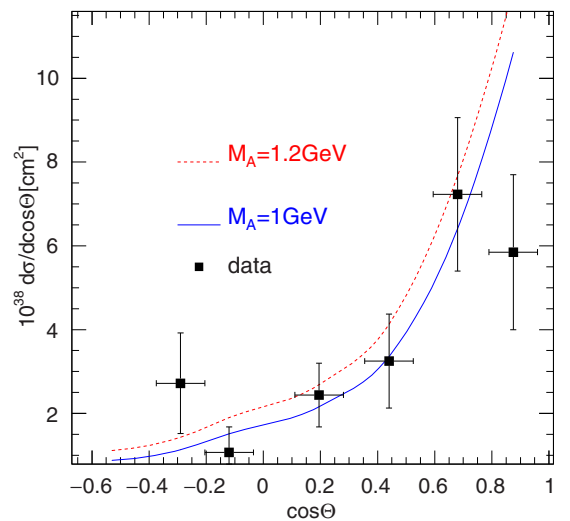

FIG. 4. The flux integrated single differential $d\sigma/d\cos\theta$ cross section as a function of the cosine of the measured muon scattering angle. Error bars show the total (statistical and systematic) uncertainty at 68% confidence level. The colored lines show the results of the RDWIA calculation with $M_A = 1$ GeV and 1.2 GeV.
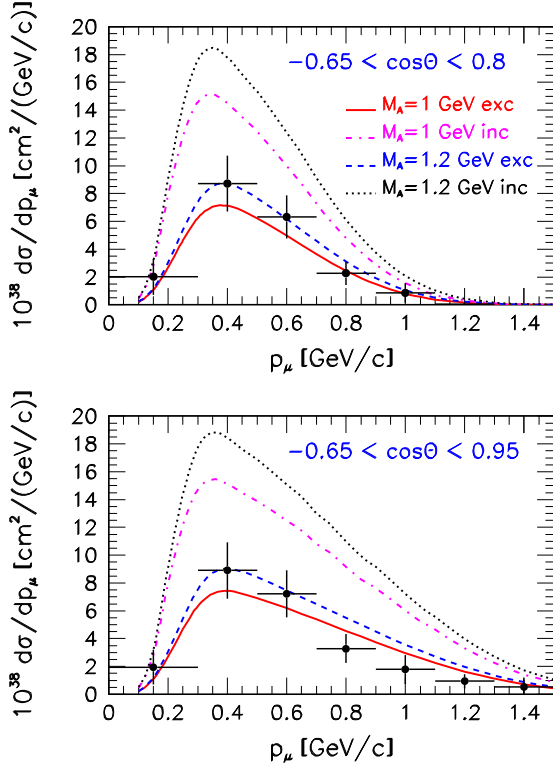
FIG. 5. The flux-integrated differential $d\sigma/dp_\mu$ cross section as a function of muon momentum. Cross sections are shown for events with $\cos\theta < 0.8$ (top) and for the full measured phase space (bottom). Error bars show the total uncertainty at 1σ confidence level. As shown in the key the semiexclusive (solid and dashed lines) and inclusive (dash-dotted and dotted lines) cross sections were calculated with $M_A = 1$ GeV and 1.2 GeV.
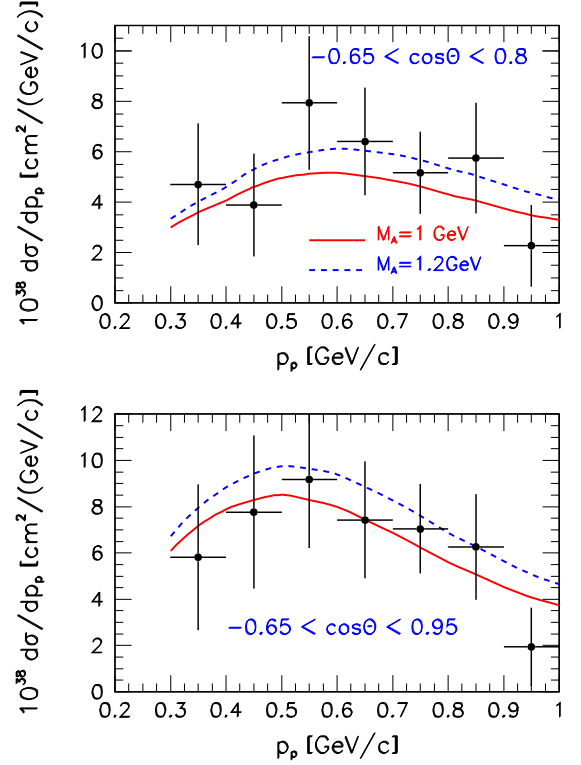

FIG. 6. The flux-integrated differential $d\sigma/dp_p$ cross section as a function of proton momentum. Cross sections are shown for events with $\cos\theta < 0.8$ (top) and without the $\cos\theta > 0.8$ requirement. Figure 6 (bottom). Error bars show the total uncertainty at 1σ confidence level. Colored lines show the results of the RDWIA calculations with $M_A = 1$ GeV and 1.2 GeV.

are presented. Figure 5 shows measured differential $d\sigma/dp_\mu$ cross section as a function of muon momentum for $-0.65 < \cos\theta < 0.95$ and $-0.65 < \cos\theta < 0.8$ compared to the RDWIA calculations. Removing events with $\cos\theta > 0.8$ significantly improves the agreement between data and theory at $p_\mu > 0.6$ GeV/c. The calculated flux-integrated cross sections for inclusive reaction are shown as well in Fig. 5 for the full measured phase space and for events with $\cos\theta < 0.8$. The contribution of $(\nu_\mu, \mu p)$ channel with $p_p > 300$ MeV/c to the inclusive $d\sigma/dp_\mu$ cross section increases slowly from 35% at $p_\mu \approx 0.2$ GeV/c to 50% at $p_\mu \approx 1$ GeV/c. The value of muon momentum where the maximum of $d\sigma/dp_\mu$ cross sections appears is about 0.4 GeV/c.

The differential cross sections $d\sigma/dp_p$ as functions of proton momentum are shown in Fig. 6 with and without events with $\cos\theta > 0.8$. Also shown are the results obtained in the RDWIA. Overall, agreement is observed between data and calculations, even for the full event sample without the $\cos\theta > 0.8$ requirement. Figure 6 demonstrates that the measured proton momentum distribution is wider than the muon momentum distribution and the maximum in the $d\sigma/dp_\mu$ cross section is located at $p_p = 0.5$ GeV/c.

Finally, Fig. 7 shows the flux-integrated differential $d\sigma/dQ^2$ cross sections as functions of Q^2 for $-0.65 <$

$\cos\theta < 0.95$ and $-0.65 < \cos\theta < 0.8$. The data are compared to the RDWIA calculations. Note, that in the bin $0.17 < Q^2 < 0.34$ (GeV/c)^2 the agreement between data and theoretical result for the full phase space is better than for event sample with the $\cos\theta$ requirement. As can be seen in Fig. 7 at $Q^2 < 0.1$ (GeV/c)^2, the measured cross section is significantly lower than the theoretical prediction. Note, that at low Q^2 the $d\sigma/dQ^2$ cross section depends weakly on the value of axial mass and Q^2 distributions are controlled by nuclear effects.

The χ^2 value for the agreement of the RDWIA prediction with data is calculated as a simple sum of those χ^2 values obtained for $d\sigma/d\cos\theta$, $d\sigma/dp_\mu$, and $d\sigma/dQ^2$ distributions separately. As follows from this analysis the values of χ^2/degree of freedom (d.o.f.) for $M_A = 1(1.2)$ GeV are χ^2/d.o.f. $= 1.12 (1.36)$ for $\cos\theta < 0.8$ and χ^2/d.o.f. $= 1.26$ (2.22) for $\cos\theta < 0.95$. The measured integrated cross sections obtained by integrating $d\sigma/d\cos\theta$ cross section over $-0.64 < \cos\theta < 0.8$ and $-0.64 < \cos\theta < 0.95$ are equal to $(4.05 \pm 1.4) \times 10^{-38}$cm^2 and $(4.93 \pm 1.55) \times 10^{-38}$ cm^2, correspondingly [13]. The calculated with $M_A = 1(1.2)$ GeV cross section values of $3.65 \times 10^{-38}(4.48 \times 10^{-38})$cm^2 for $\cos\theta < 0.8$ and $5.24 \times 10^{-38}(6.30 \times 10^{-38})$cm^2 for the full measured phase space agree also with data. On the other hand the statistical and systematic precision of the MicroBooNE data are insufficient for current needs. Thus, within
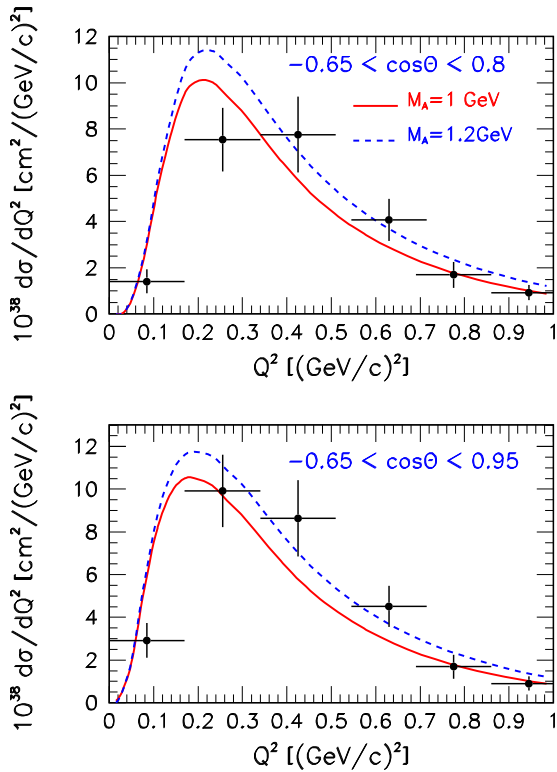
FIG. 7. As Fig. 6, but for the differential $d\sigma/dQ^2$ cross section as a function of Q^2.

the RDWIA approach the measured flux-integrated CC1p0π differential and integral cross sections can be described well within the experimental errors with $1 < M_A < 1.2$ GeV. These values of M_A are in agreement with the best fit values $M_A = 1.15 \pm 0.03$ GeV and $M_A = 1.2 \pm 0.06$ GeV obtained from the CCQE-like fit of the MiniBooNE and MINERvA

data in Refs. [53,54]. To modeling electron and muon neutrino in Ref. [55] the "MicroBooNE Tune" value of $M_A = 1.1 \pm 0.1$ GeV is used in the GENIE generator, whereas the post-ND280-fit value of $M_A = 1.13 \pm 0.08$ GeV is applied in the NEUT model [56].

IV. CONCLUSIONS

In this work I study the semiexclusive CCQE ν_μ ^{40}Ar scattering. Within the RDWIA approach the flux-integrated CC1p0π differential and integral cross sections were calculated with $M_A = 1$ GeV and 1.2 GeV. It was shown that the maximum of the double differential cross sections is in the range $0.9 < p_\mu < 1.1$ GeV and $0.8 < \cos\theta < 0.95$. The calculated single differential cross sections were tested against the MicroBooNE data. I found that the muon angular distribution is in overall agreement with measured one except at small muon scattering angle, where the measured cross section is about 2σ lower than the theoretical predictions.

The differential cross sections calculated in the RDWIA approach with $M_A = 1$ GeV and 1.2 GeV for $\cos\theta < 0.8$, and with $M_A = 1$ GeV for full phase space are in agreement with data. The calculated integral CC1p0π cross sections also agree with data even for the full event sample without the $\cos\theta < 0.8$ requirement. The contribution of the exclusive $(\nu_\mu, \mu p)$ channel with $p_p > 300$ MeV/c to the inclusive cross sections is about 50% at $p_p = 1$ GeV/c. The measurements of the double and single differential exclusive CC1p0π cross sections on ^{40}Ar with statistical and systematical uncertainty better than 20% allow to constrains models of the CCQE interaction and values of M_A that use in precision neutrino oscillation analysis.

ACKNOWLEDGMENT

[1] M. A. Acero *et al.* (NOvA Collaboration), Phys. Rev. Lett. **123**, 151803 (2019).

[2] K. Abe *et al.* (T2K Collaboration), Phys. Rev. D **103**, L011101 (2021).

[3] R. Acciarri *et al.* (DUNE Collaboration), FERMILAB-DESIGN-2016-03.

[4] K. Abe *et al.* (Hyper-Kamiokande Collaboration), arXiv:1805.04163 [physics.ins-det].

[5] M. A. Acero *et al.* (NOvA Collaboration), Phys. Rev. D **98**, 032012 (2018).

[6] A. A. Aguilar-Arevalo *et al.* (MiniBooNE Collaboration), Phys. Rev. D **81**, 092005 (2010).

[7] K. Abe *et al.* (T2K Collaboration), Phys. Rev. D **92**, 112003 (2015).

[8] G. A. Fiorentini *et al.* (MINERvA Collaboration), Phys. Rev. Lett. **111**, 022502 (2013).

[9] T. Walton *et al.* (MINERvA Collaboration), Phys. Rev. D **91**, 071301 (2015).

[10] M. Betancourt *et al.* (MINERvA Collaboration), Phys. Rev. Lett. **119**, 082001 (2017).

[11] K. Abe *et al.* (T2K Collaboration), Phys. Rev. D **98**, 032003 (2018)

[12] P. Abratenko *et al.* (MicroBooNE Collaboration) Phys. Rev. Lett. **123**, 131801 (2019).

[13] P. Abratenko *et al.* (MicroBooNE Collaboration) Phys. Rev. Lett. **125**, 201803 (2020).

[14] P. Abratenko *et al.* (MicroBooNE Collaboration) Phys. Rev. D **102**, 112013 (2020).

[15] M. Antonello *et al.* (MicroBooNe, LAr1-ND, ICARUS-WA104 Collaboration), arXiv:1503.01520 [physics.ins-det].

[16] S. Frullani and J. Mougey, Adv. Nucl. Phys. **14**, 1 (1984).

[17] A. E. L. Dieperink and P. K. A. Huberts, Annu. Rev. Nucl. Part. Sci. **40**, 239 (1990).

[18] K. G. Fissum *et al.*, Phys. Rev. C **70**, 034606 (2004)

[19] D. Dutta *et al.*, Phys. Rev. C **68**, 064603 (2003).

[20] L. Gu *et al.*, Phys. Rev. C **103**, 034604 (2021).

[21] K. Nakamura, S. Hiramatsu, T. Kamae, H. Muramatsu, H. Izutsu, and Y. Watase, Phys. Rev. Lett. **33**, 853 (1974).

[22] K. Nakamura, S. Hiramatsu, T. Kamae, H. Muramatsu, H. Izutsu, and Y. Watase, Nucl. Phys. A **271**, 221 (1976).

[23] J. Mougey, M. Bernheim, A. Bussiere, A. Gillibert, Xuan Ho Phan, M. Priou, D. Royer, I. Sick, and G. J. Wagner, Nucl. Phys. A **262**, 461 (1976).

[24] G. J. Kramer, https://inis.iaea.org/search/search.aspx?orig_q=RN:22024992.

[25] G. J. Kramer *et al.*, Phys. Lett. B **227**, 199 (1989).

[26] G. J. Kramer, H. P. Blok, and L. Lapikas, Nucl. Phys. A **679**, 267 (2001).

[27] J. J. Kelly, Adv. Nucl. Phys. **23**, 75 (1996).

[28] J. M. Udias, J. A. Caballero, E. Moya de Guerra, Javier R. Vignote, and A. Escuderos, Phys. Rev. C **64**, 024614 (2001)

[29] J. J. Kelly, Phys. Rev. C **71**, 064610 (2005).

[30] C. Maieron, M. C. Martinez, J. A. Caballero, and J. M. Udias, Phys. Rev. C **68**, 048501 (2003).

[31] A. Meucci, C. Giusti, and F. D. Pacati, Nucl. Phys. A **739**, 277 (2004).

[32] M. C. Martinez, P. Lava, N. Jachowicz, J. Ryckebusch, K. Vantournhout, and J. M. Udias, Phys. Rev. C **73**, 024607 (2006).

[33] A. Picklesimer, J. W. Van Orden, and S. J. Wallace, Phys. Rev. C **32**, 1312 (1985).

[34] A. Picklesimer and J. W. Van Orden, Phys. Rev. C **35**, 266 (1987).

[35] J. J. Kelly, Phys. Rev. C **59**, 3256 (1999).

[36] R. González-Jiménez, M. B. Barbaro, J. A. Caballero, T. W. Donnelly, N. Jachowicz, G. D. Megias, K. Niewczas, A. Nikolakopoulos, J. W. Van Orden, and J. M. Udias, arXiv:2104.01701 [nucl-th]

[37] J. E. Amaro, M. B. Barbaro, J. A. Caballero, T. W. Donnelly, R. Gonzalez-Jimenez, G. D. Megias, I. Ruiz Simo, Eur. Phys. J. Spec. Top. (2021), doi:10.1140/epjs/s11734-021-00289-5.

[38] E. B. Martinez, A. Mariano, and C. Barbero, Phys. Rev. C **103**, 015503 (2021).

[39] A. A. Aguilar-Arevalo *et al.* (MiniBooNE Collaboration), Phys. Rev. D **79**, 072002 (2009).

[40] A. V. Butkevich and S. A. Kulagin, Phys. Rev. C **76**, 045502 (2007).

[41] A. V. Butkevich, Phys. Rev. C **80**, 014610 (2009).

[42] A. V. Butkevich, Phys. Rev. C **82**, 055501 (2010).

[43] A. V. Butkevich, Phys. Rev. C **85**, 065501 (2012).

[44] A. V. Butkevich and S. V. Luchuk, Phys. Rev. C **97**, 045502 (2018).

[45] A. V. Butkevich and S. V. Luchuk, Phys. Rev. C **102**, 024602 (2020).

[46] T. de Forest, Nucl. Phys. A **392**, 232 (1983).

[47] P. Mergell, U.-G. Meissner, and D. Drechesel, Nucl. Phys. A **596**, 367 (1996).

[48] C. J. Horowitz and Brian D. Serot, Nucl. Phys. A **368**, 503 (1981).

[49] C. J. Horowitz, D. P. Murdock, and Brian D. Serot, in *Computational Nuclear Physics 1: Nuclear Structure* edited by K. Langanke, J. A. Maruhn, and Steven E. Koonin (Springer-Verlag, Berlin, 1991), p. 129.

[50] J. J. Kelly, http://www.physics.umd.edu/enp/jjkelly/LEA.

[51] E.D. Cooper, S. Hama, B. C. Clark, and R. L. Mercer, Phys. Rev. C **47**, 297 (1993).

[52] C. Ciofi degli Atti and S. Simula, Phys. Rev. C **53**, 1689 (1996).

[53] C. Wilkinson, R. Terri, C. Andreopoulos, A. Bercellie, C. Bronner, S. Cartwright, P. de Perio, J. Dobson, K. Duffy, A. P. Furmanski, L. Haegel, Y. Hayato, A. Kaboth, K. Mahn, K. S. McFarland, J. Nowak, A. Redij, P. Rodrigues, F. Sanchez, J. D. Schwehr *et al.*, Phys. Rev. D **93**, 072010 (2016).

[54] A. V. Butkevich and S. V. Luchuk, Phys. Rev. D **99**, 093001 (2019)

[55] P. Abratenko *et al.* (MicroBooNE Collaboration), arXiv:2110.14028 [hep-ex].

[56] K. Abe *et al.* (T2K Collaboration), Phys. Rev. D **103**, 112008 (2021).